IBRACON Structures and Materials Journal
Revista IBRACON de Estruturas e Materiais
ISSN 1983-4195 ismj.org

ORIGINAL ARTICLE

The influence of cracks on the corrosion initiation time caused by chloride diffusion in concrete structures using the Boundary Element Method

Influência de fissuras no tempo de iniciação da corrosão causada por difusão de cloretos em estruturas de concreto usando o Método dos Elementos de Contorno

Vinícius de Barros Souza[a]
Edson Denner Leonel[a]

[a]Universidade de São Paulo – USP, Escola de Engenharia de São Carlos, Departamento de Engenharia de Estruturas, São Carlos, SP, Brasil

Received January 09 2024
Revised August 19 2024
Accepted October 01 2024

Abstract: Reinforced concrete structures in coastal zones are subject to corrosion triggered by chloride ions. In contact with the concrete surface, such ions penetrate through the material's porous microstructure, mainly by diffusion, and accumulate on the reinforcement's surface, promoting a local breakage of the passive layer. In the classic structural service life model, the time span between the structure's exposure to chloride ions and the reinforcement depassivation is called corrosion initiation time, which may be drastically reduced in cracked concrete. Aiming to estimate the corrosion initiation time, this study uses the two-dimensional transient formulation of the Boundary Element Method (BEM) to model the chloride diffusion in reinforced concrete parts with pre-existing cracks. In this approach, different crack lengths are simulated using the subregion technique, whose crack thickness is not required. The reinforcements are represented by circular voids with nil flux in the boundary. In a rectangular beam cross-section, cracks up to 60 mm long were simulated from the concrete cover. Based on the cases studied, the influence of concrete cracking on corrosion initiation time is more significant for cracks over 20 mm long, although this result may vary depending on the position of the crack relative to the reinforcement.

Keywords: corrosion initiation time, chloride diffusion, reinforced concrete, crack, boundary element method.

Resumo: Estruturas de concreto armado situadas em zonas costeiras estão sujeitas à corrosão desencadeada por íons cloreto. Em contato com a superfície do concreto, esses íons penetram na microestrutura porosa do material, principalmente por difusão, e se acumulam na superfície da armadura, onde promovem a ruptura local da camada passivante. No modelo clássico de vida útil estrutural, o intervalo de tempo entre a exposição da estrutura aos íons cloreto e a despassivação da armadura é denominado tempo de iniciação da corrosão, o qual pode ser drasticamente reduzido em concretos fissurados. Visando estimar o tempo de iniciação da corrosão, este estudo emprega a formulação bidimensional transiente do Método dos Elementos de Contorno (MEC) para modelar a difusão de cloretos em peças de concreto armado com fissuras pré-existentes. Nessa abordagem, diferentes comprimentos de fissura são simulados por meio da técnica de sub-regiões, cuja espessura da fissura não é requerida. As armaduras são representadas por vazios circulares com fluxo nulo no contorno. Em uma viga de seção retangular foram simuladas fissuras com até 60 mm de comprimento, a partir do cobrimento de concreto. Com base nos casos estudados, a influência da fissuração do concreto no tempo de iniciação da corrosão é mais significativa para fissuras com comprimento superior a 20 mm, embora esse resultado possa variar dependendo da posição da fissura em relação à armadura.

Palavras-chave: tempo de iniciação da corrosão, difusão de cloreto, concreto armado, fissura, método dos elementos de contorno.

How to cite: V. B. Souza and E. D. Leonel, "The influence of cracks on the corrosion initiation time caused by chloride diffusion in concrete structures using the Boundary Element Method," *Rev. IBRACON Estrut. Mater.*, vol. 18, no. 1, e18108, 2025, https://doi.org/10.1590/S1983-41952025000800008.

Corresponding author: Vinícius de Barros Souza. E-mail: vbarros@usp.br
Financial support: Coordenação de Aperfeiçoamento de Pessoal de Nível Superior - Brasil (CAPES) – Finance Code 001.
Conflict of interest: Nothing to declare.
Data Availability: The data that support the findings of this study are available from the corresponding author, Souza, V. B., upon reasonable request.

1 INTRODUCTION

Reinforcement corrosion triggered by the action of chloride ions (Cl^-) is one of the main causes of deterioration of reinforced concrete (RC) structures [1]–[5]. This type of corrosion occurs mostly in coastal regions due to the structure's exposure to chloride originating from seawater by direct contact, splash zones or airborne sea salt. Chloride ions may also originate from deicing salt, industrial water, and chemical components used in the treatment of pool water.

In Brazil, reinforcement corrosion is a common pathological manifestation [6]–[8], especially in large urban centers located on the country's extensive coastline. Such observation may be highlighted in the Northeast region, where eight of its nine main cities are located in the coastal zone, the so-called urban marine environment. According to Helene [9], the velocity of corrosion may accelerate 30 to 40 times in this environment when compared to the rural atmosphere, which is considered pure.

The classic theoretical service life model of RC structures subjected to corrosion was proposed by Tuutti [10], who divided it into two consecutive stages: initiation and propagation. The first stage corresponds to the time required for carbon dioxide or chloride ions to penetrate the concrete and trigger the steel depassivation, while the second stage involves the onset and evolution of corrosion to a maximum acceptable depth. The propagation stage may develop relatively quickly compared to the former due to the effects of progressive damage caused by the corrosion products [11]–[13]. Therefore, the present study adopts the corrosion initiation time to define structural service life. Although this definition represents a conservative approach, the corrosion initiation time is a crucial parameter for the maintenance and deterioration control of RC structures [14], [15].

Besides the environment influence, the start of corrosion may be accelerated by pathological manifestation, such as the cracking concrete process. The cracks are caused by numerous solicitations, for instance, shrinkage and tensile stress due to moisture and temperature gradients [16], mechanical loading, as well as the deficient cure of concrete or concreting failure. In the case of RC structures, the superficial cracked zone may act as a preferred route of chloride ions toward the reinforcements, reducing the corrosion initiation time [17]–[20]. According to Bentz et al. [21], most service life predictions assume that the concrete will not crack or that any cracking will be immediately and effectively repaired. Disregarding the effects of cracking in the concrete may overestimate its service life in the project of structural durability [22].

Many studies have investigated and quantified the influence of cracking and its characteristics, such as depth, width, geometry (tortuosity), connectivity, and surface roughness on the chloride diffusion properties of concrete from experimental studies and numerical simulations [18], [20], [23]–[32], even though only a few have quantitatively evaluated its influence on the corrosion initiation time. Şahmaran [33] used mortar specimens with different crack widths immersed in sodium chloride solution in order to evaluate the effect of transversal cracks on the transport properties of chloride in mortar. Results have pointed out that cracks may accelerate the start of corrosion, especially when the crack width is larger than 0.135 mm. Also, in the experimental field, the study conducted by Vidal et al. [34], using elements of reinforced concrete stored in a chloride environment for 17 years, reported that transversal cracks, developed by bending, with a width inferior to 0.40 mm, do not have a significant influence on the structural service life. However, according to the experimental results presented by Otieno et al. [35], depending on the quality and the type of concrete, a crack width inferior to 0.40 mm may significantly affect the beginning and propagation of corrosion on RC structures.

Ghanooni-Bagha et al. [16] simulated different crack's depths and thicknesses in the center of a concrete part, using multiphysics modeling via the Finite Element Method (FEM). The period of time for the level of chloride, at a point near the crack and 50 mm distant from the surface exposed to chloride ions, to reach half of the superficial concentration was 50 days for concrete with cracks of 0.1 mm and 0.5 mm wide, and 50 mm length. In contrast, the same level of chloride was reached in 500 days in sound concrete [16].

Peng et al. [20] modeled a five-phase material to represent the heterogeneity of concrete, including a damaged zone and different crack patterns. Tapered, tortuous, and parallel-wall cracks were modeled through the cross-section, but relatively slight differences have been observed in the chloride concentration profiles [20]. Although tortuosity can affect chloride diffusivity, its influence is less important in small cracks. Bentz et al. [21] simulated a proposition of repair for the concrete cracking and a damaged zone surrounding the crack. When the repair strategy is applied only to the crack, the damaged zone turns into a new region of material fragility, reducing service life by up to 82% when compared to sound concrete.

Numerical modeling of cracks on concrete, associated with chloride diffusion is of great relevance in the engineering area for replacing relatively costly experimental studies. Despite the fact that cracks are idealized in most of the numerical models, the incorporation of its influence in the chloride diffusion on RC structures has an important role regarding the prediction of structural service life as well as defining structural maintenance actions.

The BEM has been applied to solve fracture mechanics problems within solid mechanics for more than four decades. There are some well-known approaches based on boundary integral equations to deal with fracture mechanics. One of

them is the so-called Dual BEM [36], which applies two distinct integral equations for the solution of the problem. A singular equation is written for elements defined on one side of the crack surface and a second (hypersingular) equation is written for the opposite crack face. This scheme eliminates singularities in the final system of equations, which arise from the singular nature of the fundamental solutions. Another approach is the dipole BEM formulation [37]. This strategy introduces self-equilibrated virtual forces on the crack boundaries, called dipoles, originating an initial stress field able to correct the cohesive stresses on the crack surfaces and to represent the fracture process zone. Both Dual and dipole BEM formulations are efficient for simulating the crack growth [38], [39], although the latter requires only the discretization of one crack surface. Crouch [40] proposed the Displacement Discontinuity Method (DDM) for plane elasticity problems, which also discretizes solely one side of the crack surface. The DDM is a kind of indirect BEM that uses hypersingular integral equations to accurately model crack propagation [39]. Based on the best of the authors' knowledge, the BEM hypersingular formulation for transient potential problems is not known yet, which prevents the application of the mentioned approaches in problems of transient diffusion. Alternatively, the subregion technique can be applied to such a proposal.

The subregion technique was initially proposed to represent non-homogeneous domains [41]. Blandford et al. [42] first used this technique to discretize cracked surfaces, attesting to its accuracy and efficiency. The idea aims to divide the original domain into subregions such that the crack face belongs to adjacent regions. Hence, the subregion technique requires discretization of both sides of the crack faces. Then, equilibrium and compatibility conditions are enforced on the non-cracked interfaces to guarantee their continuity. Modifying those conditions to boundary conditions yields the crack growth simulation. The global system of equations is obtained by assembling the boundary element formulation written for each subregion [43]. Shao et al. [44] have demonstrated the application of this technique to simulate the propagation of cohesive cracks in concrete beams. According to these authors [44], the technique can provide agreeable results based on comparison against experimental measures. Other research works can be cited [45]–[55], most of them devoted to solid mechanic problems. In the diffusion field, the applications are still incipient, or non-existent in some cases.

In the present study, the subregion technique is coupled to the two-dimensional (2D) potential transient formulation of the BEM for modeling RC cracked structures exposed to chloride attack. The BEM modeling may provide computational savings regarding the problem representation, as the method does not require a domain mesh, but a boundary mesh. Despite this, internal fields to the boundary can be determined with high precision. Herein, the boundary discretization uses isoparametric Lagrangian elements with any order of approximation. On the other hand, interpolation of temporal quantities uses linear functions to represent complex boundary conditions varying over time. In this latter scheme, regular internal kernels are numerically solved by Gauss-Legendre quadrature, while singular kernels are treated by the Singularity Subtraction technique [56].

Assuming that the diffusivity of concrete is steady in time, this study seeks to evaluate the influence of the crack length on the corrosion initiation time for RC structures exposed to a coastal atmosphere. Cracks are idealized assuming straight shape and fixed depth, and the chloride concentration throughout its length is the same as the connected external surface.

Since the reinforcement does influence the flux of chlorides due to the accumulation of these ions around the rebar's surface, the steel bars in the cross-section are represented as circular holes with no flux on their boundaries [21], [57], i.e., resistant to chloride diffusion. Even though the representation of crack and rebar are idealized, the model provides predictions of corrosion initiation time that may be useful in the service life project of RC structures, replacing oversimplified analytical models.

2 THE BEM FORMULATION

2.1 The transient potential problem

The differential equation that governs the transient potential problem is (Equation 1):

$$\nabla^2 u - \frac{1}{k}\frac{\partial u}{\partial t} = 0, \tag{1}$$

in which u represents potential, t refers to the time variable, and k is the diffusion coefficient.

The definition of the problem is complete with the imposition of boundary conditions in potential and flux (q), and initial conditions in the domain, respectively (Equations 2, 3 and 4):

$$u(x,t) = \bar{u}(x,t)\ x \in \Gamma_1, \tag{2}$$

$$q(x,t) = \bar{q}(x,t)\ x \in \Gamma_2, \tag{3}$$

$$u(x,t_0) = u_0(x)\ x \in \Omega, \tag{4}$$

where u_0 is the potential described in the domain (Ω), in the initial time (t_0). $\bar{u}$ and $\bar{q}$ represent the values of prescribed potential in Γ_1 and prescribed flux in Γ_2, respectively, in which $\Gamma = \Gamma_1 \cup \Gamma_2$ stands for the boundary of the domain.

The q flux in the structure surface is determined by the u directional derivative regarding the normal vector to the boundary (η), meaning $q = \partial u/\partial \eta$. In the context of the present study, the potential represents the chloride concentration in such a position and instant of time, while q represents the chloride flux in the concrete.

The differential equation in expression (1) may be transformed into an integral equation using time-dependent fundamental solutions. The fundamental problem that originates the fundamental solutions is characterized by a semi-infinite domain subject to a punctual source applied in time t_0, represented by the Dirac delta function. In addition to the time variable, these fundamental solutions are described in a field point function (x) and a source point (ξ). In the point ξ, the application of the source is represented by the Dirac delta function, while x is the point where it is desired to measure and quantify the influence of the source. For two-dimensional cases, fundamental solutions in terms of potential (u^*) and flux (q^*), respectively, are defined by [58] (Equations 5 and 6):

$$u^*(\xi,x,t_F,t) = \frac{1}{4\pi k\tau} exp\left(-\frac{r^2}{4k\tau}\right), \tag{5}$$

$$q^*(\xi,x,t_F,t) = -\frac{r\frac{\partial r}{\partial \eta}}{8\pi k^2\tau^2} exp\left(-\frac{r^2}{4k\tau}\right), \tag{6}$$

in which $\tau = t_F - t$, where t_F stands for the time of analysis, r is the distance between the source point and the field point, and $\frac{\partial r}{\partial \eta} = r_{,k}\,\eta_k$.

By integrating Equation 1 in the whole domain of analysis and the time interval $[t_0,\ t_F]$, considering fundamental solutions as weight functions and a series of algebraic manipulations, including the application of the weighted residuals technique, integration by parts, and the limit process to take the source point to the boundary, the following integral equation is provided [58]:

$$c(\xi)u(\xi,t_F) + \int_{t_0}^{t_F}\int_{\Gamma} u(x,t)\ q^*(\xi,x,t_F,t)k\ d\Gamma\ dt = \int_{t_0}^{t_F}\int_{\Gamma} q(x,t)\ u^*(\xi,x,t_F,t)k\ d\Gamma\ dt + \int_{\Omega} u_0(x)\ q^*(\xi,x,t_F,t_0)k\ d\Omega \tag{7}$$

in which $c(\xi)$ is the free term, whose value is function of the source point position. In the cases in which the source point is located on the smooth boundary, $c(\xi) = 0.5$ is given.

Equation 7 presents a domain integral that may be transformed into a boundary integral through the Dual Reciprocity Method. However, it is assumed here that $u_0 = 0$, which implicates in the nil source of potential in the domain at the beginning of the analysis. In practice, this consideration indicates that the concrete was fabricated without any component containing chloride in its composition, as required by the Brazilian standard NBR 6118 [59]. Besides, it is assumed that the diffusion coefficient (k) is steady in time and space. Given such assumptions, Equation 7 is rewritten as:

$$c(\xi)u(\xi,t_F) + k\int_{t_0}^{t_F}\int_{\Gamma} u(x,t)\ q^*(\xi,x,t_F,t)d\Gamma dt = k\int_{t_0}^{t_F}\int_{\Gamma} q(x,t)\ u^*(\xi,x,t_F,t)d\Gamma dt \tag{8}$$

2.2 Numerical solution

The numerical solution of Equation 8 demands spatial and temporal discretization. Therefore, the geometric boundary is discretized in NE Langrangian isoparametric elements with any order of approximation, and the time span $t_F - t_0$ in NT steps of uniformed size. A time-stepping scheme using linear interpolation functions is applied, enabling the analytical evaluation of time-dependent BEM's integral kernels.

By inverting the order of integration in Equation 8 and by introducing Lagrangian polynomials (ϕ) for the interpolation of boundary Γ, one provides:

$$c_i\, u_{i,NT} + k \sum_{j=1}^{NE} \sum_{p=1}^{NT} \int_{\Gamma_j} \phi_j \int_{t_{p-1}}^{t_p} u\, q^* dt\, d\Gamma_j = k \sum_{j=1}^{NE} \sum_{p=1}^{NT} \int_{\Gamma_j} \phi_j \int_{t_{p-1}}^{t_p} q\, u^* dt\, d\Gamma_j \tag{9}$$

in which $u_{i,NT}$ refers to the potential value in the source point i at $p = NT$.

The linear temporal interpolation functions are given by (Equations 10 and 11):

$$u(t) = \frac{(t-t_{p-1})u_{j,p} + (t_p - t)u_{j,p-1}}{\Delta t} \tag{10}$$

$$q(t) = \frac{(t-t_{p-1})q_{j,p} + (t_p - t)q_{j,p-1}}{\Delta t} \tag{11}$$

with $\Delta t = t_p - t_{p-1}$.

By replacing Equations 10 and 11 in Equation 9, to the time span $t_{p-1} \leq t \leq t_p$, the order of the sums is inverted so that:

$$c_i\, u_{i,NT} + \sum_{p=1}^{NT} \sum_{j=1}^{NE} \left(H_{ij,p}^1 u_{j,p-1} + \hat{H}_{ij,p}^2 u_{j,p} \right) = \sum_{p=1}^{NT} \sum_{j=1}^{NE} \left(G_{ij,p}^1 q_{j,p-1} + G_{ij,p}^2 q_{j,p} \right) \tag{12}$$

in which:

$$H_{ij,p}^1 = \frac{k}{\Delta t} \int_{\Gamma_j} \phi_j \int_{t_{p-1}}^{t_p} (t_p - t)\, q^* dt\, d\Gamma_j \tag{13a}$$

$$\hat{H}_{ij,p}^2 = \frac{k}{\Delta t} \int_{\Gamma_j} \phi_j \int_{t_{p-1}}^{t_p} (t - t_{p-1})\, q^* dt\, d\Gamma_j \tag{13b}$$

$$G_{ij,p}^1 = \frac{k}{\Delta t} \int_{\Gamma_j} \phi_j \int_{t_{p-1}}^{t_p} (t_p - t)\, u^* dt\, d\Gamma_j \tag{13c}$$

$$G_{ij,p}^2 = \frac{k}{\Delta t} \int_{\Gamma_j} \phi_j \int_{t_{p-1}}^{t_p} (t - t_{p-1})\, u^* dt\, d\Gamma_j \tag{13d}$$

The analytical solution of the time integral kernels in Equations 13a-d are given as follows [58] (Equations 14 to 17):

$$\int_{t_{p-1}}^{t_p} (t_p - t)\, q^* dt = \frac{1}{2\pi k} \frac{\partial r}{\partial \eta} \left\{ \frac{(t_F - t_p)}{r} \left[exp\,(-\alpha_{p-1}) - exp\,(-\alpha_p) \right] - \frac{r}{4k} \left[E_1(\alpha_{p-1}) - E_1(\alpha_p) \right] \right\} \tag{14}$$

$$\int_{t_{p-1}}^{t_p} (t - t_{p-1})\, q^* dt = \frac{1}{2\pi k} \frac{\partial r}{\partial \eta} \left\{ \frac{(t_F - t_{p-1})}{r} \left[exp\,(-\alpha_p) - exp\,(-\alpha_{p-1}) \right] + \frac{r}{4k} \left[E_1(\alpha_{p-1}) - E_1(\alpha_p) \right] \right\} \tag{15}$$

$$\int_{t_{p-1}}^{t_p} (t_p - t) u^* dt = \frac{1}{4\pi k} \left\{ \left(t_p - t_F - \frac{r^2}{4k} \right) \left[E_1(\alpha_{p-1}) - E_1(\alpha_p) \right] + \frac{r^2}{4k} \left[\frac{exp\,(-\alpha_{p-1})}{\alpha_{p-1}} - \frac{exp\,(-\alpha_p)}{\alpha_p} \right] \right\} \tag{16}$$

$$\int_{t_{p-1}}^{t_p} (t - t_{p-1}) u^* dt = \frac{1}{4\pi k} \left\{ \left(t_F - t_{p-1} + \frac{r^2}{4k} \right) \left[E_1(\alpha_{p-1}) - E_1(\alpha_p) \right] + \frac{r^2}{4k} \left[\frac{exp\,(-\alpha_p)}{\alpha_p} - \frac{exp\,(-\alpha_{p-1})}{\alpha_{p-1}} \right] \right\} \tag{17}$$

in which $\alpha_{p-1} = \frac{r^2}{4k(t_F - t_{p-1})}$, $\alpha_p = \frac{r^2}{4k(t_F - t_p)}$ and E_1 is the exponential integral function.

The boundary integrals are numerically evaluated by the Gauss-Legendre quadrature with the exception of $G_{ii,1}^2$ kernel that must be evaluated in the sense of Cauchy Principal Value for presenting a singular behavior [56].

By considering the source point over the smooth boundaries, Equation 12 may be written in the following compact form:

$$H_{ij,p}^{1} u_{j,p-1} + H_{ij,p}^{2} u_{j,p} = G_{ij,p}^{1} q_{j,p-1} + G_{ij,p}^{2} q_{j,p} \tag{18}$$

Where (Equation 19):

$$H_{ij,p}^{2} = \begin{cases} \widehat{H}_{ij,p}^{2} + 0{,}5 \; if \; i = j \; e \; p = 1, \\ \widehat{H}_{ij,p}^{2} \; otherwise. \end{cases} \tag{19}$$

By applying Equation 18 for each i node of the boundary, the following algebraic representation is obtained [60]:

$$\sum_{p=1}^{NT} ([H^1]^{NT-p} + [H^2]^{NT-p+1}) \{u\}^p = \sum_{p=1}^{NT} ([G^1]^{NT-p} + [G^2]^{NT-p+1}) \{q\}^p \tag{20}$$

The solution for Equation 20 involves the classic scheme of BEM's column change procedure. This scheme seeks to algebraically enforce the exchange of components between $\{u\}^p$ and $\{q\}^p$ which results in the $\{f\}^p$ and $\{x\}^p$ vectors of prescribed and unknown quantities in the boundary, respectively, for each time step. Thus, the system of linear equations is given by (Equation 21):

$$[A]\{x\}^p = [B]\{f\}^p + \sum_{n=1}^{p-1} \{([G^1]^{p-n} + [G^2]^{p-n+1})\{q\}^n + ([H^1]^{p-n} + [H^2]^{p-n+1})\{u\}^n\} \tag{21}$$

in which $[A]$ and $[B]$ matrices are obtained with the columns change procedure between $[G^2]$ and $[H^2]$ matrices in the first time step.

Once the quantities in the boundaries are known, the potential in internal points of the domain is computed by Equation 12, attributing $c_i = 1.0$, which is rewritten as follows:

$$u_{i,NT} + \sum_{p=1}^{NT} \sum_{j=1}^{NE} \left(H_{ij,p}^{1} u_{j,p-1} + \widehat{H}_{ij,p}^{2} u_{j,p} \right) = \sum_{p=1}^{NT} \sum_{j=1}^{NE} \left(G_{ij,p}^{1} q_{j,p-1} + G_{ij,p}^{2} q_{j,p} \right) \tag{22}$$

Integral kernels in Equation 22 are evaluated considering the position of the source point internally to the domain, and numerically solved once singularities do not occur. In the compact form, the potential vector at internal points $\{u_{int}\}$ is explicitly written as:

$$\{u_{int}\} = \sum_{p=1}^{NT} \left(([G^1]^{NT-p} + [G^2]^{NT-p+1})\{q\}^p - ([H^1]^{NT-p} + [H^2]^{NT-p+1})\{u\}^p \right) \tag{23}$$

2.2 Application 1 - Chloride diffusion in a cylindrical RC specimen

In order to verify the accuracy of the numerical model previously described, the results provided via BEM are compared to those reported by Arora et al. [57] in the semi-analytical solution of a reinforced concrete part submitted to the radial diffusion process. The cylindrical specimen has concrete cover e around a rebar of radius r_1 = 0.5 cm, as depicted in Figure 1a. The reinforcement is represented by a circular hole with nil flux prescribed in the boundary [57].

For a period of 1,400 days of exposition, it is assumed that the chloride concentration in the part's surface exponentially increases in time (t) as it is expressed [57]: $C_s(t) = C_0[1 - \exp(-at)]$, in which C_0 is the equilibrium concentration of chloride ions at the surface of concrete (% of cement mass) and a stands for the empirical adsorption parameter (s^{-1}).

This problem is two-dimensionally represented by a region of thickness e between two concentric circumferences (Figure 1b). Both Γ_1 e Γ_2 boundaries of the cross-section geometry were discretized with 12 isoparametric Lagrangian elements of quadratic order (72 nodes).

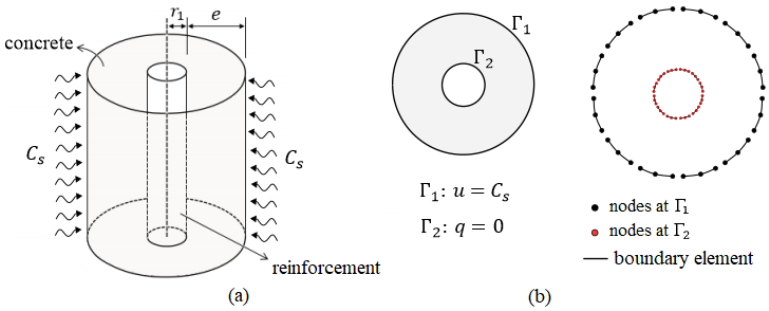

Figure 1. a) Specimen geometry, b) 2D mesh and boundary conditions.

It is assumed that C_0=2.40%, a=1.16x10^{-7} s^{-1} (10.02x10^{-3} day^{-1}), k = 4x10^{-8} cm^2/s [57], and e equal 2.5 cm, 3.5 cm, and 4.5 cm. Figure 2 compares the chloride profiles obtained by Arora et al. [57] against the present study, which adopted 10 Gauss points per boundary element and time increments of 2 days.

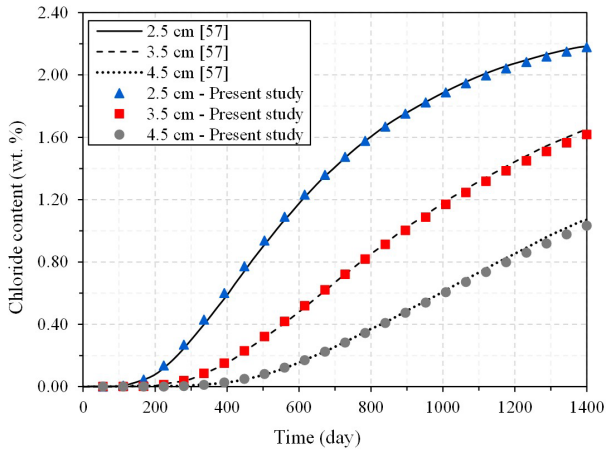

Figure 2. Chloride profiles for reinforced concrete cylinders of different thickness.

Figure 2 shows good correspondence between the semi-analytical response and the transient potential BEM solution. Taking into account 0.20% of chloride ions as threshold concentration for reinforcement depassivation, Arora et al. [57] present a corrosion initiation time of 263 days (e=2.5 cm), 437 days (e=3.5 cm), and 652 days (e=4.5cm). For these same thicknesses, BEM's solution provides 254 days, 428 days, and 648 days, respectively. Although the latter is more conservative, these results lead to a percentage difference of less than 3.50%, attesting the accuracy of the presented formulation.

2.3 Subregion technique

The BEM's subregion technique allows the representation of non-homogeneous domains as multiply-connected materials [41]. The domain is divided into piecewise homogeneous portions, which are bonded by enforcing compatibility and equilibrium conditions among material interfaces. Regarding the potential problem, such conditions are defined by:

$$u_i^s = u_i^z \tag{24}$$

$$q_i^s = -q_i^z \tag{25}$$

in which u_i stands potential and q_i flux at node i. The superscript index refers to the subregion to which the interface's node i belongs, with $s \neq z$.

By simplicity, considering a domain discretized into two subregions (Figure 3), the algebraic system given by Equation 20 is independently applied for each subregion. Combining these systems of equations in sparse matrices provides the following global algebraic representation:

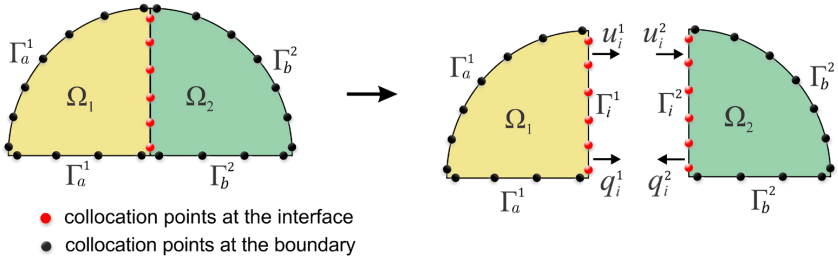

Figure 3. Discretization of a non-homogeneous domain into subregions.

$$\begin{bmatrix} H_a^1 & H_i^1 & 0 & 0 \\ 0 & 0 & H_b^2 & H_i^2 \end{bmatrix} \begin{Bmatrix} u_a^1 \\ u_i^1 \\ u_b^2 \\ u_i^2 \end{Bmatrix} = \begin{bmatrix} G_a^1 & G_i^1 & 0 & 0 \\ 0 & 0 & G_b^2 & G_i^2 \end{bmatrix} \begin{Bmatrix} q_a^1 \\ q_i^1 \\ q_b^2 \\ q_i^2 \end{Bmatrix} \tag{26}$$

Applying the equilibrium of flux and compatibility of potentials among interface's node i of subregions 1 and 2 (Equations 24 and 25), considering $s = 1$ and $z = 2$, Equation 26 is simplified to:

$$\begin{bmatrix} H_a^1 & H_i^1 & 0 \\ 0 & H_i^2 & H_b^2 \end{bmatrix} \begin{Bmatrix} u_a^1 \\ u_i^1 \\ u_b^2 \end{Bmatrix} = \begin{bmatrix} G_a^1 & G_i^1 & 0 \\ 0 & -G_i^2 & G_b^2 \end{bmatrix} \begin{Bmatrix} q_a^1 \\ q_i^1 \\ q_b^2 \end{Bmatrix} \tag{27}$$

The solution of Equation 27 provides the unknown quantities at the boundary nodes and at the interfaces among subregions through the exchange of terms between matrices and vectors. For nodes located inside the subregion, the potential is computed by Equation 23, considering only the system of equations of the subregion to which the node belongs, i.e., each subregion is solved as an independent domain.

The subregion technique can also be applied to represent geometric discontinuities, such as coplanar surface cracks. In this approach, artificial boundaries are introduced into the domain, so that each of the interfaces among subregions contains a crack surface [61]. Continuity among adjacent subregions is ensured by enforcing compatibility and equilibrium conditions relative to the type of problem assessed, whereas boundary conditions are prescribed in the nodes that discretize the crack. As stated by Blandford et al. [42], this technique avoids matrix singularity problems since the crack surfaces are independently represented in each domain. Figure 4 illustrates the discretization of crack geometry using the subregion technique.

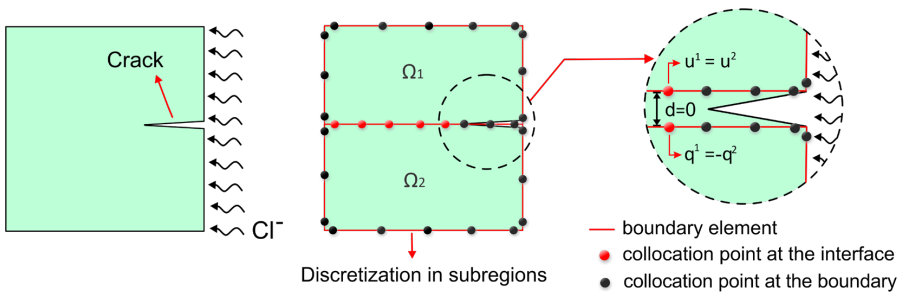

Figure 4. Representation of cracks by the subregion technique.

It is worth noting that this approach does not require a diffusion coefficient in the cracked zone, since the crack is discretely considered in the analysis. On the other hand, it is necessary to prescribe the chloride concentration at the

crack's boundary, which may be a drawback considering that this data is difficult to determine in practice and may considerably change from the superficial concentration on the external surface connected to the crack.

Formulations previously presented were implemented in computational subroutines using the FORTRAN 90 programming language. The final code provides the numerical solution of transient potential problems through 2D BEM in a non-homogeneous and cracked body.

3 NUMERICAL APPLICATIONS

3.1 Application 2 - The effect of cracking on chloride diffusion in concrete

The influence of cracks on chloride penetration in concrete is verified by comparing BEM's predictions to results obtained by Marsavina et al. [24], who performed an experimental study on specimens of non-carbonated concrete mixes (Portland cement content of 400 kg/m^3) with artificial cracks (notches). In this experiment, the cracks were produced by inserting and removing thin copper sheets inside the concrete, resulting in a single crack in the symmetric axis of each specimen.

The specimens, with 100 mm in diameter and 50 mm in thickness, were submitted to a non-steady state migration test, described in NT BUILD 492 [62]. An external electrical potential of 25 V was applied across the specimen for a limited time duration, forcing chloride ions from the 10% NaCl solution (22.045 kg/m^3 Cl^-) to migrate into the concrete [24]. The experimental program was carried out in intervals of 2h, 4h, 6h, 8h, and 10h, in which three specimens were tested for each of these time periods. After each test, the specimens were axially split perpendicularly to the notch and sprayed with AgNO3 solution. The chloride penetration depth was measured at 15 points, corresponding to the concentration at which the AgNO3 solution changed color (1.183 kg/m^3 of Cl^-).

For the numerical simulation of the test, we adopted a two-dimensional model of rectangular geometry, measuring 100 mm x 50 mm (Figure 5a), with a central crack of 0.3 mm width and 20 mm depth. Based on the specimen tested for 10 hours, the diffusion coefficient in sound concrete was adopted as $24.51\text{x}10^{-12}$ m^2/s [63]. To determine the exposure time equivalent to a natural diffusion, the solution of the differential equation of Fick's Second Law [64] – Equation 28 – was applied as a function of the superficial chloride concentration (24.045 kg/m^3) and the average penetration depth experimentally obtained at the ends of the concrete samples, which corresponds to a chloride content of 1.183 kg/m^3 [24].

$$t = \frac{1}{4k_0}\left[\frac{x}{\text{erfc}^{-1}\left(\frac{C_x}{C_s}\right)}\right]^2, \tag{28}$$

in which k_0 stands for the steady diffusion coefficient, erfc refers to Gauss' complementary error function, C_s is the superficial concentration, and C_x is the chloride concentration at depth x.

The boundary mesh used in this analysis comprises two subregions, each discretized with 40 isoparametric Lagrangian elements of quadratic approximation and 84 nodes. The crack has been modeled as a straight line 20 mm long in the center of the cross-section, where the two subregions are conjoined (Figure 5b). On the surface in contact with the crack, the chloride concentration is 24.045 kg/m^3 [24] and nil on the opposite side. The lateral surfaces were sealed with rubber, ensuring watertight, which is represented by the imposition of nil chloride flux in these boundaries. As considered in Šavija et al. [63], we assume that the chloride concentration at the notch is the same as the bottom surface.

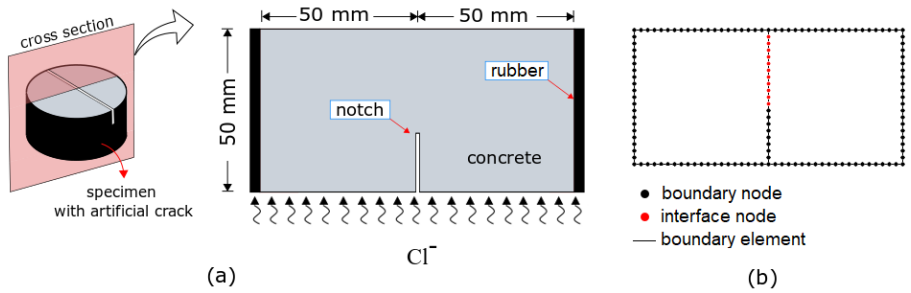

Figure 5. a) Two-dimensional representation of geometry, b) Boundary mesh.

Figure 6 presents the average penetration profiles corresponding to the concentration of 1.183 kg/m^3 of chloride per exposure time. For the numerical results (BEM), 111 time steps were adopted and a grid of 4,563 internal points distributed in the domain whose results were interpolated, considering a variation of ±0.04 kg/m^3.

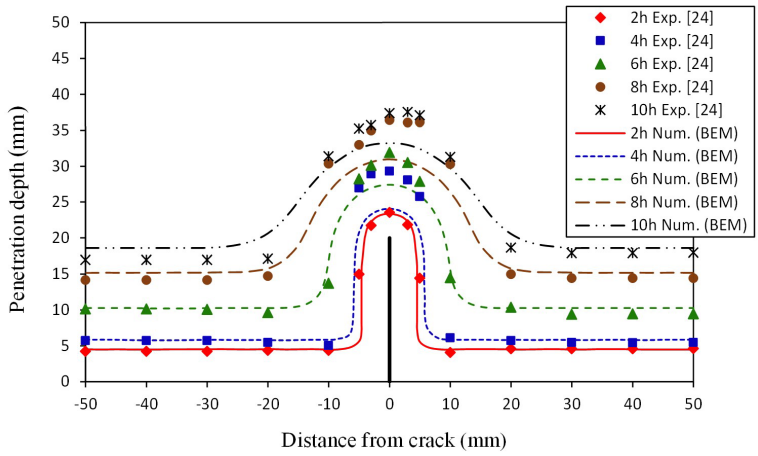

Figure 6. Chloride penetration depth in concrete with a notch width 0.3 mm and 20 mm long: a comparison between experimental [24] and numerical results (present study).

Based on Figure 6, there is a good correspondence between the experimental and numerical results in the sound concrete regions, mainly for the curves referring to the exposure time of 2, 4, and 6 hours. As expected, chloride penetration in the vicinity of the notch is higher than in the other regions of the specimen. However, around the notch tip, only the 2-hour simulation agrees with the experimental result. For longer exposure times, the accelerated migration test provides a deeper and narrower penetration front than the BEM numerical predictions.

Šavija et al. [63] points out a fundamental reason why migration tests provide sharper and narrower penetration profiles than pure diffusion. According to them, the applied voltage in the migration test increases the mobility of the chloride ions only in the longitudinal direction. The higher the voltage, the more accentuated is the penetration front at the notch tip, which makes it more complex to correlate accelerated migration tests to natural conditions [63]. These authors also cite a wall effect that might have caused a more porous zone close to the notch, increasing the penetration front during the experiment [63]. According to Marsavina et al. [24], the higher depth of penetration close to the notch can also be correlated to possible microcracks, for instance, due to hydration and shrinkage of the concrete in the experimental test, whose effects were not considered in the present numerical analysis.

Figure 7 presents the chloride profiles numerically assessed with the two-dimensional BEM model. Following the behavior of the curves in Figure 6, the concentration profiles become smoother and more uniform as the exposure time to chloride ions increases, expanding the area of influence around the damaged zone.

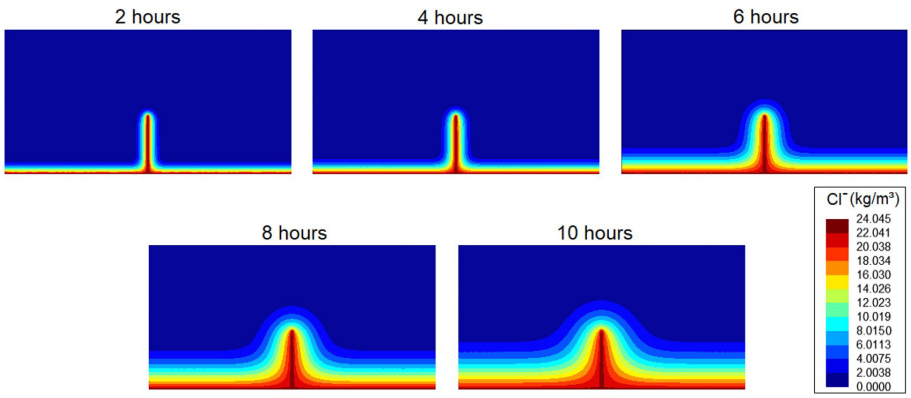

Figure 7. Penetration of chloride ions (Cl^-) in concrete specimen with a central notch of 20 mm depth over different exposure times.

3.2 Application 3 - The influence of cracks on corrosion initiation time

In order to investigate the influence of cracks on corrosion initiation time, two cracks were considered in the tensile zone of an RC beam – Figure 8 – whose cross-section has dimensions of 200 mm x 300 mm. The beam is reinforced with five rebars of 20 mm in diameter and two rebars of 8 mm in diameter. For the sake of simplicity, the transverse reinforcement (stirrup) was not represented in the model, so the concrete cover (CC) is considered the shortest distance from the beam surface to the rebar's boundary.

The variation of chloride concentration on the lateral and bottom surfaces of the beam is governed by the expression $C_s(t) = C_0[1 - \exp(-0.25t)]$, in which t is the evaluated time in years, and $C_0 = 2.95$ kg/m^3 the mean superficial content in coastal zones [65], [66]. The top beam surface is conjoined to the rest of the structure. Therefore it is not directly exposed to the coastal atmosphere. This condition is represented by the imposition of nil chloride flux through the upper boundary.

The cracks are straight and appear in pairs of same length, 50 mm apart. Six crack lengths have been simulated: 10 mm, 20 mm, 30 mm, 40 mm, 50 mm, and 60 mm. It is assumed that the chloride concentration on the surface of the cracks varies in time according to C_s.

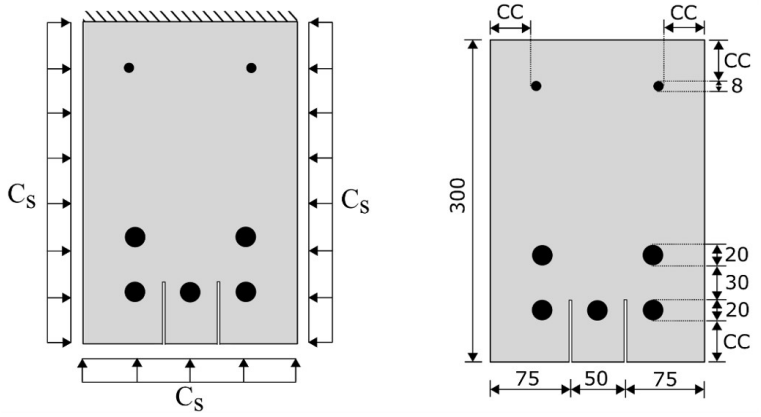

Figure 8. Cross-section geometry (dimensions in mm) and boundary conditions.

The boundary mesh, with quadratic approximation, is composed of two subregions: 55 isoparametric Lagrangian elements discretize the subregion between the cracks, including the center rebar, and 154 isoparametric Lagrangian elements discretize the remaining boundaries and reinforcements; totaling 430 nodes. Once again, the reinforcements are represented as circular holes with nil flux prescribed in the boundary. For numerical integration, 10 Gauss points and 80 time steps have been adopted.

The diffusion coefficient of the concrete is determined by the following empirical equation [67]: $k(w/c) = 10^{-10+4.66(w/c)}$cm^2/s, in which w/c stands for the water to cement ratio in the concrete mixture. An estimate of the *w/c* ratio is obtained through the concrete compressive strength, f_{ck} (in MPa), using Bolomey's formula [66] (Equation 29):

$$w/c = \frac{27}{f_{ck}+13.5}. \tag{29}$$

Taking into account that the beam is already cracked at the beginning of exposure to the coastal atmosphere, Figure 9 presents the maximum chloride concentration at the rebar surface over a 20-year period, considering six different beam designs:

- Design 1: $f_{ck} = 45$ MPa and CC = 25 mm;
- Design 2: $f_{ck} = 45$ MPa and CC = 30 mm;
- Design 3: $f_{ck} = 45$ MPa and CC = 40 mm;
- Design 4: $f_{ck} = 45$ MPa and CC = 45 mm;
- Design 5: $f_{ck} = 45$ MPa and CC = 50 mm;
- Design 6: $f_{ck} = 50$ MPa and CC = 40 mm.

We clarify that the results in Figure 9 do not represent the behavior of a specific point on the reinforcement. Each curve shows the highest chloride concentration measured among all rebars, for each time step. The corrosion initiation time is considered the lowest time span in which the chloride concentration at the reinforcement reaches an average of 0.90 kg/m^3 for its depassivation [67]. This threshold content is highlighted by the dashed line in Figure 9.

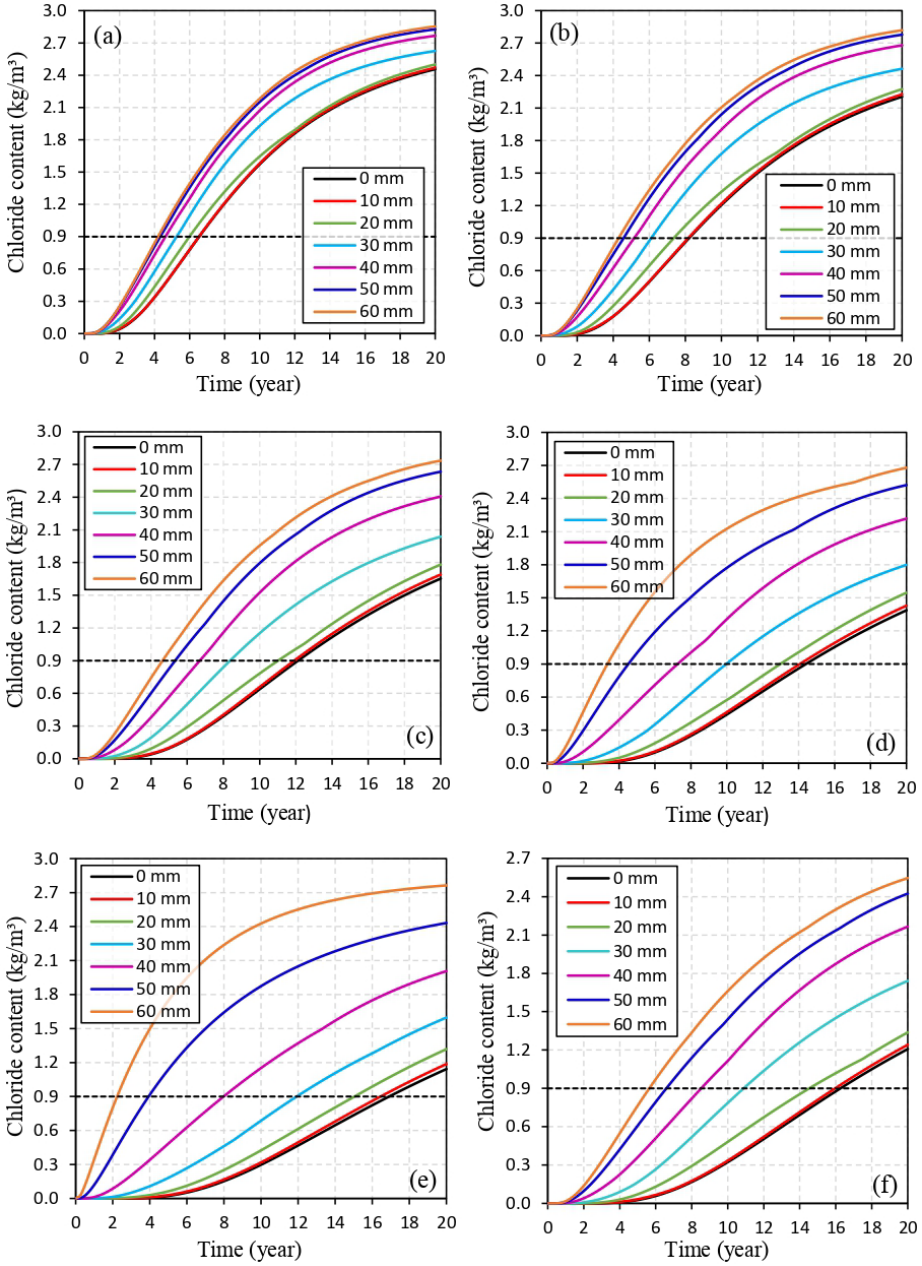

Figure 9. Maximum chloride concentration on the rebar surface for different crack lengths: a) design 1, b) design 2, c) design 3, d) design 4, e) design 5, and f) design 6.

Overall, Figure 9 demonstrates that the behavior of curves regarding cracks up to 20 mm long remains close to the sound beam curve (0 mm). A more significant decrease in corrosion initiation time occurs from 30 mm crack length. Fo the sake of comparison, Table 1 summarizes the corrosion initiation time corresponding to the chloride threshold content of 0.90 kg/m^3 for each design configuration previously mentioned.

Table 1. Corrosion initiation time for sound and cracked RC beam with different design configurations.

Crack length (mm)	Corrosion initiation time (year)					
	Design 1	Design 2	Design 3	Design 4	Design 5	Design 6
0	6.500	8.250	12.125	14.500	17.000	16.250
10	6.500	8.200	12.000	14.125	16.500	16.000
20	6.000	7.375	11.000	13.000	15.000	14.500
30	5.250	6.125	8.375	10.000	11.950	10.875
40	4.625	5.125	6.750	7.250	8.000	8.500
50	4.370	4.450	5.375	4.500	3.950	6.625
60	4.200	4.300	4.625	3.375	2.250	5.625

Designs 1 and 2 correspond to 25 mm and 30 mm concrete covers, respectively. The Brazilian Association of Technical Standards [59] recommends a minimum concrete cover of 40 mm for highly aggressive environments (class III - Marine). Therefore, the first two design configurations represent critical cases that contradict Brazilian technical recommendations. Comparing these cases with design 3, in which the concrete has a 40 mm cover and the same compressive strength, a substantial increase in the structural service life can be noted, especially for cases with cracks of up to 20 mm length. Based on data from design 3, a 50 mm long cracks would reduce the beam service life by more than half compared to the same sound structure.

Taking design 3 as a reference, two dimensioning strategies were defined: an increase in the concrete cover, and an increase in the concrete compressive strength. The first strategy increases the concrete cover to 45 mm (design 4) and 50 mm (design 5), while maintaining the concrete compressive strength of 45 MPa. In the second strategy, the cover depth is set to 40 mm, while the concrete strength is increased to 50 MPa. The graphical results are shown in Figure 9d-f.

Regarding the first strategy, the increase of concrete cover delayed the reinforcement depassivation for cracks up to 40 mm in length. However, for crack lengths of 50 mm and 60 mm, this strategy led to a drastic reduction in corrosion initiation time. In the case of idealized cracks simulated here, these results may be justified by the position of the cracks relative to the reinforcements. Ghanooni-Bagha et al. [16] corroborate that the greatest depth of chloride ingress in a specific region and at different time intervals is not necessarily caused by cracks of greater thickness and depth, but based on the correspondence between the crack depth and the position of the reinforcements in the concrete matrix.

On the other hand, the increase of the concrete compressive strength was the most assertive strategy for the cases with crack lengths of 40 mm, 50 mm, and 60 mm, since design 6 delayed the corrosion initiation time for this crack range. Certainly, these results are subject to variations depending on the position of the crack and reinforcements.

Taking into account that structural systems are designed to achieve a service life of at least 50 years [68], the results in Table 1 are relatively short. However, it is worth stressing that a conservative service life model has been adopted, based on the depassivation of the reinforcements. Hence, it does not mean that the structure is subject to imminent failure, but that the corrosion process is due to start. For the structural engineering applications, these estimates can be used, for example, as reference measures to define inspection and maintenance programs of RC structures located in highly aggressive atmospheres, such as the urban marine environment, in order to prevent or delay the need for rehabilitation of a corroded structural element.

Figure 10 graphically correlates the crack length and corrosion initiation time using data from Table 1 and those provided by simulating intermediate crack lengths (5 mm, 15 mm, 25 mm, 35 mm, 45 mm, and 55 mm). Overall, the curves present a steeper slope for cracks longer than 20 mm. In other words, crack lengths up to 20 mm do not pose a high risk of accelerating the corrosion initiation time. Based on Figure 10, for concrete compressive strength of 45 MPa and 40 mm cover depth (design 3), the average reduction in corrosion initiation time is 0.28 years for every 5 mm of increase in crack length up to 20 mm, while for longer cracks (25 to 60 mm), the corrosion initiation time decreases 0.80 years, in average, for every 5 mm added to the crack length.

For design 3, Figures 11 to 13 present the distribution maps of chlorides to the sound and cracked RC beam during 6 years, 12 years, and 20 years of exposure to the coastal atmosphere, respectively. It can be noted that the chloride concentration varies spatially around the rebars, which leads to spatial variation in the corrosion initiation time. Thus, the reinforcement surfaces nearest the crack tip reach the threshold content for depassivation more quickly than other regions. This statement reinforces the position of the crack as a key parameter to accelerate the corrosion initiation time. In sound concrete, however, the chloride content for steel depassivation is more likely to be reached first in the reinforcements near to the beam corners due to the bidirectional flux of these ions.

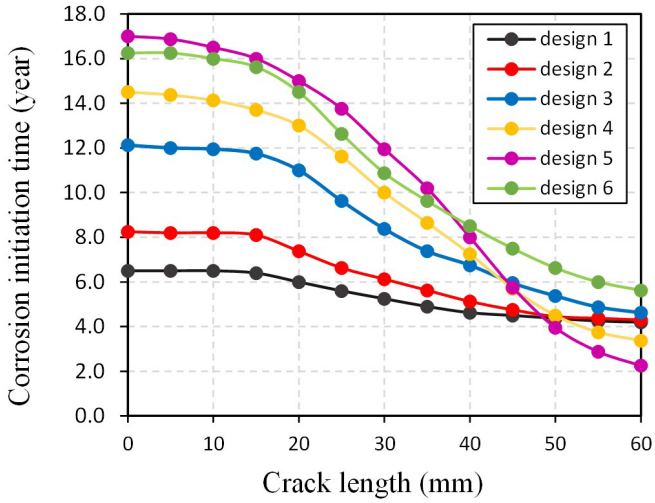

Figure 10. Crack length versus corrosion initiation time for different beam designs.

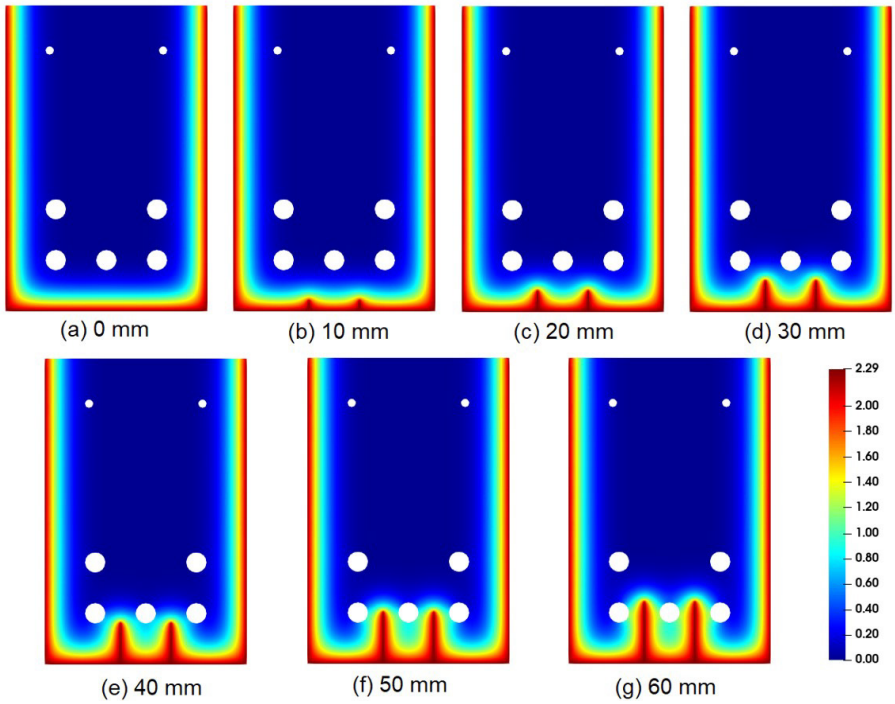

Figure 11. Chloride concentration distribution (kg/m^3) at 6 years in beam design 3 for different crack lengths.

It is important to note that the phenomenon of chloride diffusion in real-world structures is subject to randomness, which can affect the representativeness of deterministic results. For instance, the empirical equation adopted in application 3 to determine the diffusion coefficient in concrete considers solely the influence of the water to cement ratio. In fact, the diffusivity of concrete can depend on various factors, such as the mix proportion (w/c ratio, type of cement, levels of fly ash and slag, aggregate/cement ratio) [67], concrete age, curing, compaction, temperature, degree of hydration, relative humidity of the pores, time of exposure to a chloride environment etc. There is a range of expressions proposed in the literature to represent the permeability of concrete [69]–[77], which may lead to minor or major variations in the presented results. In this context, it is strongly recommended that the analysis of chloride diffusion in concrete takes structural reliability into account.

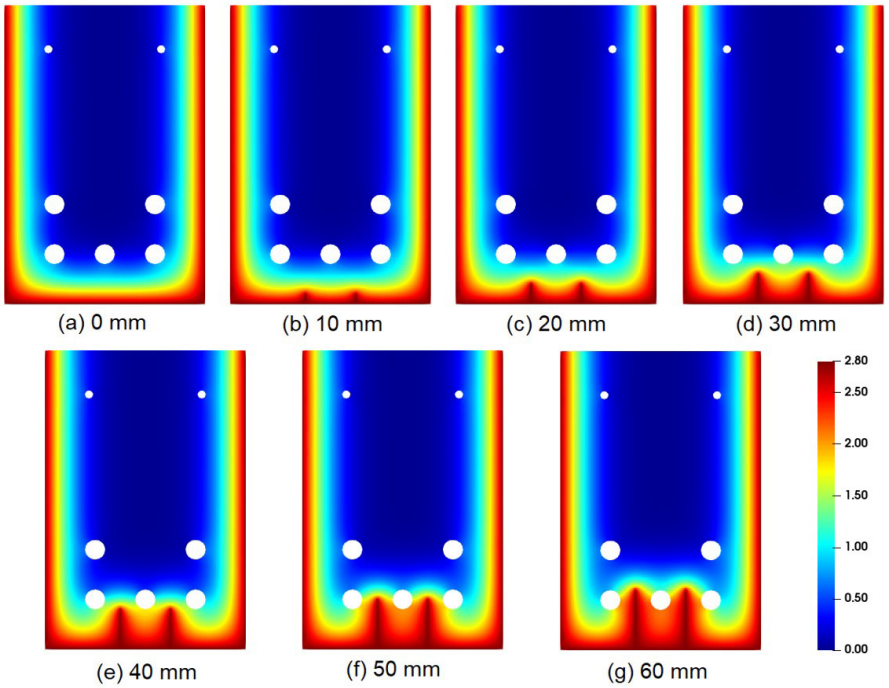

Figure 12. Chloride concentration distribution (kg/m^3) at 12 years in beam design 3 for different crack lengths.

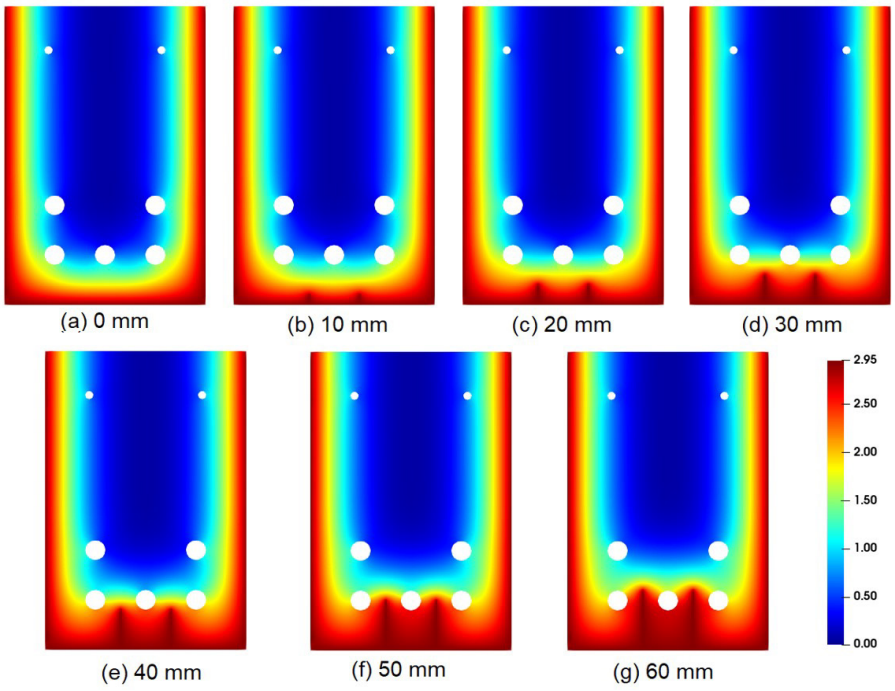

Figure 13. Chloride concentration distribution (kg/m^3) at 20 years in beam design 3 for different crack lengths.

4 CONCLUSIONS

In this study, concrete structures with steady time diffusivity have been numerically simulated by 2D BEM's transient formulation to evaluate the influence of pre-existing cracks on the corrosion initiation time. It was assumed that the cracks have an idealized shape and the chloride concentration along their length is the same as that of the external surface connected to the crack. Based on the numerical simulations, the following conclusions can be drawn:

- In comparison to the experimental non-steady state migration test, one verifies a difference of results near the notch tip, possibly due to the voltage applied in the migration test to accelerate the chloride migration through the concrete. This effect was not considered in the present formulation, which underestimated the chloride penetration depths over the notch tip, except for the 2-hour exposure test. However, in the sound concrete regions, all numerical simulations agreed relatively well with the experimental measurements;
- In the beam cross-section of 200 mm x 300 mm, the crack lengths up to 20 mm do not exert considerable influence on the reduction of corrosion initiation time. In the specific case of concrete with 40 mm cover depth and compressive strength of 45 MPa, cracks up to 20 mm led to an average reduction of 0.28 years in the corrosion initiation time for every 5 mm added to the crack length, against 0.80 years for cracks of superior length (up to 60 mm);
- The position and the length of the crack are crucial features for the penetration of chlorides towards the reinforcement, since the increase of the concrete cover did not necessarily delayed the corrosion initiation time for all crack lengths simulated in the RC beam;
- Regarding the mechanical model, the use of linear temporal integration provided good accuracy in predicting the corrosion initiation time and allowed the adequate description of the superficial chloride concentration with complex variation in time. In addition, the subregion technique enabled to represent different cracks lengths using the same boundary mesh. Nevertheless, this model can still be improved in further works, extending, for example, the formulation to the three-dimensional approach, where the influence of crack thickness can be represented.

ACKNOWLEDGEMENTS

The authors gratefully acknowledge Coordination of Superior Level Staff Improvement – Brazil (CAPES) – Finance Code 001, for the financial support provided.

REFERENCES

[1] D. V. Val, L. Chernin, and M. G. Stewart, "Experimental and numerical investigation of corrosion-induced cover cracking in reinforced concrete structures," *J. Struct. Eng.*, vol. 135, no. 4, pp. 376–385, Apr 2009, http://doi.org/10.1061/(ASCE)0733-9445(2009)135:4(376).

[2] S. Muthulingam and B. N. Rao, "Non-uniform time-to-corrosion initiation in steel reinforced concrete under chloride environment," *Corros. Sci.*, vol. 82, pp. 304–315, May 2014, http://doi.org/10.1016/j.corsci.2014.01.023.

[3] E. Bastidas-Arteaga and F. Schoefs, " Sustainable maintenance and repair of RC coastal structures," *Proc. Inst. Civ. Engineers-Maritime Eng.*, vol. 168, no. 4, pp. 162–173, Dec 2015, http://doi.org/10.1680/jmaen.14.00018.

[4] M. Shakouri and D. Trejo, "A time-variant model of surface chloride build-up for improved service life predictions," *Cement Concr. Compos.*, vol. 84, pp. 99–110, Nov 2017, http://doi.org/10.1016/j.cemconcomp.2017.08.008.

[5] U. M. Angst, "Predicting the time to corrosion initiation in reinforced concrete structures exposed to chlorides," *Cement Concr. Res.*, vol. 115, pp. 559–567, Jan 2019, http://doi.org/10.1016/j.cemconres.2018.08.007.

[6] L. I. Olivan, L. Scandiuzzi, O. S. Taki, and T. D. Ferreira, "Aumento da durabilidade das estruturas de concreto usando vergalhão de aço galvanizado," in *An. INTERCORR*, Salvador - BA, May 2012.

[7] G. R. Meira, *Corrosão de Armaduras em Estruturas de Concreto: Fundamentos, Diagnóstico e Prevenção*. João Pessoa: Editora IFPB, 2017.

[8] C. B. L. Oliveira, M. Greco, and T. N. Bittencourt, "Analysis of the Brazilian federal bridge inventory," *Rev. IBRACON Estrut. Mater.*, vol. 12, no. 1, pp. 1–13, Feb 2019, http://doi.org/10.1590/s1983-41952019000100002.

[9] P. R. Helene, *Corrosão em Armaduras para Concreto Armado*, 1ª ed. São Paulo: Pini, 1986.

[10] K. Tuutti, *Corrosion of Steel in Concrete* (Report 4-82). Stockholm: Swedish Cem. Concr. Res. Inst., 1982.

[11] P. Thoft-Christensen, "Assessment of the reliability profiles for concrete bridges," *Eng. Struct.*, vol. 20, no. 11, pp. 1004–1009, Nov 1998, http://doi.org/10.1016/S0141-0296(97)00196-X.

[12] W. Y. Jung, Y.-S. Yoon, and Y.-M. Sohn, "Predicting the remaining service life of land concrete by steel corrosion," *Cement Concr. Res.*, vol. 33, no. 5, pp. 663–677, May 2003, http://doi.org/10.1016/S0008-8846(02)01034-7.

[13] M. G. Richardson, *Fundamentals of Durable Reinforced Concrete.* Boca Raton: CRC Press, Apr. 2004, http://doi.org/10.1201/9781482272109.

[14] D. V. Val and P. A. Trapper, "Probabilistic evaluation of initiation time of chloride-induced corrosion," *Reliab. Eng. Syst. Saf.*, vol. 93, no. 3, pp. 364–372, Mar 2008, http://doi.org/10.1016/j.ress.2006.12.010.

[15] J. Lizarazo-Marriaga, C. Higuera, I. Guzmán, and L. Fonseca, "Probabilistic modeling to predict fly-ash concrete corrosion initiation," *J. Build. Eng.*, vol. 30, pp. 101296, Jul 2020, http://doi.org/10.1016/j.jobe.2020.101296.

[16] M. Ghanooni-Bagha, M. A. Shayanfar, and M. H. Farnia, "Cracking effects on chloride diffusion and corrosion initiation in RC structures via finite element simulation," *Sci. Iran.*, vol. 27, no. 5, pp. 2301–2315, Sep 2020, http://doi.org/10.24200/sci.2018.50496.1725.

[17] K. Audenaert, G. D. Schutter, and L. Marsavina, "Influence of cracks and crack width on penetration depth of chlorides in concrete," *Eur. J. Environ. Civ. Eng.*, vol. 13, no. 5, pp. 561–572, Oct 2009, http://doi.org/10.1080/19648189.2009.9693134.

[18] W. Wang, Z. Tang, Z. Li, and H. Ma, "Simulation of chloride diffusion in cracked concrete with different crack patterns," *Adv. Mater. Sci. Eng.*, vol. 2016, pp. 1–11, Mar 2016, http://doi.org/10.1155/2016/7982365.

[19] F. U. A. Shaikh, "Effect of cracking on corrosion of steel in concrete," *Int. J. Concr. Struct. Mater.*, vol. 12, no. 1, pp. 3, Jan 2018, http://doi.org/10.1186/s40069-018-0234-y.

[20] J. Peng, S. Hu, J. Zhang, C. Cai, and L. Li, "Influence of cracks on chloride diffusivity in concrete: a five-phase mesoscale model approach," *Constr. Build. Mater.*, vol. 197, pp. 587–596, Feb 2019, http://doi.org/10.1016/j.conbuildmat.2018.11.208.

[21] D. P. Bentz, W. S. Guthrie, S. Z. Jones, and N. Martys, "Predicting service life of steel-reinforced concrete exposed to chlorides: a discussion of real-world considerations for effective modeling," in *ACI Concr. Int.*, Sept. 2014. Accessed: Oct. 5, 2023. [Online]. Available: https://tsapps.nist.gov/publication/get_pdf.cfm?pub_id=915806

[22] R. Zhang, L. Jin, M. Liu, X. Du, and Y. Li, "Numerical investigation of chloride diffusivity in cracked concrete," *Mag. Concr. Res.*, vol. 69, no. 16, pp. 850–864, Jul 2017, http://doi.org/10.1680/jmacr.16.00511.

[23] A. Djerbi, S. Bonnet, A. Khelidj, and V. Baroghel-Bouny, "Influence of traversing crack on chloride diffusion into concrete," *Cement Concr. Res.*, vol. 38, no. 6, pp. 877–883, Jun 2008, http://doi.org/10.1016/j.cemconres.2007.10.007.

[24] L. Marsavina, K. Audenaert, G. De Schutter, M. Faur, and D. Marsavina, "Experimental and numerical determination of the chloride penetration in cracked concrete," *Constr. Build. Mater.*, vol. 23, no. 1, pp. 264–274, Jan 2009, http://doi.org/10.1016/j.conbuildmat.2007.12.015.

[25] T. Ishida, P. O. N. Iqbal, and H. T. L. Anh, "Modeling of chloride diffusivity coupled with non-linear binding capacity in sound and cracked concrete," *Cement Concr. Res.*, vol. 39, no. 10, pp. 913–923, Oct 2009, http://doi.org/10.1016/j.cemconres.2009.07.014.

[26] L. Wang and T. Ueda, "Mesoscale modelling of the chloride diffusion in cracks and cracked concrete," *J. Adv. Concr. Technol.*, vol. 9, no. 3, pp. 241–249, Sep 2011, http://doi.org/10.3151/jact.9.241.

[27] S. S. Park, S. J. Kwon, and S. H. Jung, "Analysis technique for chloride penetration in cracked concrete using equivalent diffusion and permeation," *Constr. Build. Mater.*, vol. 29, pp. 183–192, Apr 2012, http://doi.org/10.1016/j.conbuildmat.2011.09.019.

[28] M. Rahman, W. Al-Kutti, M. Shazali, and M. Baluch, "Simulation of chloride migration in compression-induced damage in concrete," *J. Mater. Civ. Eng.*, vol. 24, no. 7, pp. 789–796, Jul 2012, http://doi.org/10.1061/(ASCE)MT.1943-5533.0000458.

[29] X. Du, L. Jin, R. Zhang, and Y. Li, "Effect of cracks on concrete diffusivity: a meso-scale numerical study," *Ocean Eng.*, vol. 108, pp. 539–551, Nov 2015, http://doi.org/10.1016/j.oceaneng.2015.08.054.

[30] H. Wang, J. Dai, X. Sun, and X. Zhang, "Characteristics of concrete cracks and their influence on chloride penetration," *Constr. Build. Mater.*, vol. 107, pp. 216–225, Mar 2016, http://doi.org/10.1016/j.conbuildmat.2016.01.002.

[31] W. Li and L. Guo, "A mechanical-diffusive peridynamics coupling model for meso-scale simulation of chloride penetration in concrete under loadings," *Constr. Build. Mater.*, vol. 241, pp. 118021, Apr 2020, http://doi.org/10.1016/j.conbuildmat.2020.118021.

[32] Q. Wang, G. Zhang, Y. Tong and C. Gu, "A numerical study on chloride diffusion in cracked concrete," *Crystals*, vol. 11, no. 7, pp. 1–11, Jun. 2021, http://doi.org/10.3390/cryst11070742.

[33] M. Şahmaran, "Effect of flexure induced transverse crack and self-healing on chloride diffusivity of reinforced mortar," *J. Mater. Sci.*, vol. 42, no. 22, pp. 9131–9136, Nov 2007, http://doi.org/10.1007/s10853-007-1932-z.

[34] T. Vidal, A. Castel, and R. François, "Corrosion process and structural performance of a 17 year old reinforced concrete beam stored in chloride environment," *Cement Concr. Res.*, vol. 37, no. 11, pp. 1551–1561, Nov 2007, http://doi.org/10.1016/j.cemconres.2007.08.004.

[35] M. B. Otieno, M. G. Alexander, and H. D. Beushausen, "Corrosion in cracked and uncracked concrete - Influence of crack width, concrete quality and crack opening," *Mag. Concr. Res.*, vol. 62, no. 6, pp. 393–404, Jun 2010, http://doi.org/10.1680/macr.2010.62.6.393.

[36] A. Portela, M. Aliabadi, and D. Rooke, "The dual boundary element method: effective implementation for crack problems," *Int. J. Numer. Methods Eng.*, vol. 33, no. 6, pp. 1269–1287, Apr 1992, http://doi.org/10.1002/nme.1620330611.

[37] F. S. Rocha and W. S. Venturini, "Boundary element algorithm to solve discontinuity problems," in *Boundary Elements X: Stress Analysis*, C. A. Brebbia, Ed., Southampton: Comp. Mech. Pub., vol. 3, pp. 107–118, 1988.

[38] R. Citarella, G. Cricrì, and E. Armentani, "Multiple crack propagation with Dual Boundary Element Method in stiffened and reinforced full scale aeronautic panels," *Key Eng. Mater.*, vol. 560, pp. 129–155, Jul 2013, http://doi.org/10.4028/www.scientific.net/KEM.560.129.

[39] L. R. P. Almeida, E. T. Lima Jr., and J. C. C. Barbirato, "Cohesive crack propagation analysis using a dipole BEM formulation with tangent operator," *Theor. Appl. Fract. Mech.*, vol. 109, pp. 102765, Oct 2020, http://doi.org/10.1016/j.tafmec.2020.102765.

[40] S. Crouch, "Solution of plane elasticity problems by the displacement discontinuity method. I. Infinite body solution," *Int. J. Numer. Methods Eng.*, vol. 10, no. 2, pp. 301–343, 1976, http://doi.org/10.1002/nme.1620100206.

[41] F. J. Rizzo and D. J. Shippy, "A formulation and solution procedure for the general non-homogeneous elastic inclusion problem," *Int. J. Solids Struct.*, vol. 4, no. 12, pp. 1161–1179, Dec 1968, http://doi.org/10.1016/0020-7683(68)90003-6.

[42] G. E. Blandford, A. R. Ingraffea, and J. A. Liggett, "Two-dimensional stress intensity factor computations using the boundary element method," *Int. J. Numer. Methods Eng.*, vol. 17, no. 3, pp. 387–404, Mar 1981, http://doi.org/10.1002/nme.1620170308.

[43] X.-W. Gao, L. Guo, and C. Zhang, "Three-step multi-domain BEM solver for nonhomogeneous material problems," *Eng. Anal. Bound. Elem.*, vol. 31, no. 12, pp. 965–973, Dec 2007, http://doi.org/10.1016/j.enganabound.2007.06.002.

[44] Y. Shao, Z. Cen, T. Li, and Z. Du, "Fracture Characteristics of concrete structures using sub-domain Boundary Element Method," *Eng. Mech.*, vol. 26, no. 8, pp. 107–115, Aug 2009.

[45] A. R. Ingraffea, G. E. Blandford, and J. A. Liggett, "Automatic modelling of mixed-mode fatigue and quasi-static crack propagation using the boundary element method," in *Proc. 14th Nat. Sym. Fract. ASTM Int.*, 1983, pp. 1407–1426.

[46] K. Y. Lee and H. J. Choi, "Boundary element analysis of stress intensity factors for bimaterial interface cracks," *Eng. Fract. Mech.*, vol. 29, no. 4, pp. 461–472, 1988, http://doi.org/10.1016/0013-7944(88)90033-1.

[47] T. Chen, B. Wang, Z. Cen, and Z. Wu, "A symmetric Galerkin multi-zone boundary element method for cohesive crack growth," *Eng. Fract. Mech.*, vol. 63, no. 5, pp. 591–609, 1999, http://doi.org/10.1016/S0013-7944(99)00036-3.

[48] X. W. Gao and M. C. He, "A new inverse analysis approach for multi-region heat conduction BEM using complex-variable-differentiation method," *Eng. Anal. Bound. Elem.*, vol. 29, no. 8, pp. 788–795, Aug 2005, http://doi.org/10.1016/j.enganabound.2005.03.001.

[49] C. Zhang, M. Cui, J. Wang, X. W. Gao, J. Sladek, and V. Sladek, "3D crack analysis in functionally graded materials," *Eng. Fract. Mech.*, vol. 78, no. 3, pp. 585–604, Feb. 2011, http://doi.org/10.1016/j.engfracmech.2010.05.017.

[50] Y. Zhao, Y. Guo, T. Miao, M. Zhao, and C. Fan, "An iterative approach for analyzing cracks in two-dimensional piezoelectric media with exact boundary conditions," *Eng. Anal. Bound. Elem.*, vol. 90, pp. 76–85, May 2018, http://doi.org/10.1016/j.enganabound.2018.01.005.

[51] V. Gnitko, K. Degtyariov, V. Naumenko, and E. Strelnikova, "BEM and FEM analysis of the fluid-structure interaction in tanks with baffles," *Inter. J. Comp. Methods Exp. Meas.*, vol. 5, no. 3, pp. 317–328, 2017, http://doi.org/10.2495/CMEM-V5-N3-317-328.

[52] E. Chen and C. K. Y. Leung, "A coupled diffusion-mechanical model with boundary element method to predict concrete cover cracking due to steel corrosion," *Corros. Sci.*, vol. 126, pp. 180–196, Sep 2017, http://doi.org/10.1016/j.corsci.2017.07.001.

[53] V. V. Gnitko, K. G. Degtyariov, A. A. Karaiev, and E. A. Strelnikova, "“Multi-domain boundary element method for axisymmetric problems in potential theory and linear isotropic elasticity," *Sci WIT Trans. Eng. Sci.*, vol. 122, pp. 13–25, 2018, http://doi.org/10.2495/BE410021.

[54] L. Igumnov and I. Markov, "Dynamic response of a structure partially embedded in anisotropic elastic half-space using BEM," *AIP Conf. Proc.*, vol. 2216, no. 1, pp. 020005, Apr 2020, http://doi.org/10.1063/5.0003572.

[55] V. B. Souza and E. D. Leonel, "Probabilistic chloride diffusion modelling in cracked concrete structures by transient BEM formulation," *Rev. IBRACON Estrut. Mater.*, vol. 15, no. 4, pp. e15402, 2022, http://doi.org/10.1590/s1983-41952022000400002.

[56] M. Guiggiani and P. Casalini, "Direct computation of Cauchy principal value integrals in advanced boundary elements," *Int. J. Numer. Methods Eng.*, vol. 24, no. 9, pp. 1711–1720, Sep 1987, http://doi.org/10.1002/nme.1620240908.

[57] P. Arora, B. N. Popov, B. Haran, M. Ramasubramanian, S. Popova, and R. E. White, "Corrosion initiation time of steel reinforcement in a chloride environment: a one dimensional solution," *Corros. Sci.*, vol. 39, no. 4, pp. 739–759, Apr 1997, http://doi.org/10.1016/S0010-938X(96)00163-1.

[58] L. C. Wrobel, *The Boundary Element Method: Applications in Thermo-Fluids and Acoustics.* United Kingdom: John Wiley & Sons, 2002, vol. 1.

[59] Associação Brasileira de Normas Técnicas, *Projeto de Estruturas de Concreto*, ABNT NBR 6118, Aug. 2023.

[60] P. K. Banerjee, *The Boundary Element Methods in Engineering*, 2nd ed. London: McGraw-Hill, 1994, 496 p.

[61] M. H. Aliabadi, *The Boundary Element Method, volume 2: Applications in Solids and Structures*, 1st ed. New York: Wiley, 2002, 636 p.

[62] Nordtest, *Concrete, Mortar and Cement-based Repair Materials: Chloride Migration Coefficient from Non-steady State Migration Experiment*, NT BUILD 492, Finland, 1999.

[63] B. Šavija, M. Luković, and E. Schlangen, "Lattice modeling of rapid chloride migration in concrete," *Cement Concr. Res.*, vol. 61, pp. 49–63, Jul 2014, http://doi.org/10.1016/j.cemconres.2014.04.004.

[64] A. Fick, "Ueber diffusion," *Ann. Phys.*," vol. 170, pp. 59–86, Jan. 1855, http://doi.org/10.1002/andp.18551700105.

[65] M. K. Kassir and M. Ghosn, "Chloride-induced corrosion of reinforced concrete bridge decks," *Cement Concr. Res.*, vol. 32, no. 1, pp. 139–143, Jan 2002, http://doi.org/10.1016/S0008-8846(01)00644-5.

[66] D. V. Val and M. G. Stewart, "Life-cycle cost analysis of reinforced concrete structures in marine environments," *Struct. Saf.*, vol. 25, no. 4, pp. 343–362, Oct 2003, http://doi.org/10.1016/S0167-4730(03)00014-6.

[67] M. G. Stewart and D. V. Rosowsky, "Structural safety and serviceability of concrete bridges subject to corrosion," *J. Infrastruct. Syst.*, vol. 4, no. 4, pp. 146–155, Dec 1998, http://doi.org/10.1061/(ASCE)1076-0342(1998)4:4(146).

[68] Associação Brasileira de Normas Técnicas, *Residential Buildings – Performance. Part 1: General Requirements, No. 4*, ABNT NBR 15575-1, Jan. 2024.

[69] A. V. Saetta, R. V. Scotta, and R. V. Vitaliani, "Analysis of chloride diffusion into partially saturated concrete," *ACI Mater. J.*, vol. 90, no. 5, pp. 441–451, 1993, http://doi.org/10.14359/3874.

[70] P. S. Mangat and B. T. Molloy, "Prediction of long term chloride concentration in concrete," *Mater. Struct.*, vol. 27, no. 6, pp. 338–346, Jul 1994, http://doi.org/10.1007/BF02473426.

[71] B. Gerard, G. Pijaudier-Cabot, and C. Laborderie, "Coupled diffusion-damage modelling and the implications on failure due to strain localisation," *Int. J. Solids Struct.*, vol. 35, no. 31-32, pp. 4107–4120, Nov 1998, http://doi.org/10.1016/S0020-7683(97)00304-1.

[72] V. G. Papadakis, "Effect of supplementary cementing materials on concrete resistance against carbonation and chloride ingress," *Cement Concr. Res.*, vol. 30, no. 2, pp. 291–299, Feb 2000, http://doi.org/10.1016/S0008-8846(99)00249-5.

[73] K. Stanish and M. Thomas, "The use of bulk diffusion tests to establish time-dependent concrete chloride diffusion coefficients," *Cement Concr. Res.*, vol. 33, no. 1, pp. 55–62, Jan 2003, http://doi.org/10.1016/S0008-8846(02)00925-0.

[74] J. Zheng and X. Zhou, "Analytical solution for the chloride diffusivity of hardened cement paste," *J. Mater. Civ. Eng.*, vol. 20, no. 5, pp. 384–391, May 2008, http://doi.org/10.1061/(ASCE)0899-1561(2008)20:5(384).

[75] A. Djerbi, S. Bonnet, A. Khelidj, and V. Baroghel-Bouny, "Influence of traversing crack on chloride diffusion into concrete," *Cement Concr. Res.*, vol. 38, no. 6, pp. 877–883, Jun 2008, http://doi.org/10.1016/j.cemconres.2007.10.007.

[76] S. Kwon, U. Na, S. Park, and S. Jung, "Service life prediction of concrete wharves with early-aged crack: probabilistic approach for chloride diffusion," *Struct. Saf.*, vol. 31, no. 1, pp. 75–83, Jan 2009, http://doi.org/10.1016/j.strusafe.2008.03.004.

[77] S. Park, S. Kwon, and S. Jung, "Analysis technique for chloride penetration in cracked concrete using equivalent diffusion and permeation," *Constr. Build. Mater.*, vol. 29, pp. 183–192, Apr 2012, http://doi.org/10.1016/j.conbuildmat.2011.09.019.

Author contributions: VBS: conceptualization, literature review, methodology, computational implementation & validation, formal analysis, written, illustration and editing. EDL: conceptualization, literature review, methodology, formal analysis, supervision, layout, writing-review.

Editors: Vladimir Haach, Daniel Cardoso.